Physics of the Microchannel Flow Boiling Process and Comparison With the Existing Theories

Sajjad Bigham
Department of Mechanical and Aerospace Engineering,
University of Florida,
Gainesville, FL 32611

Saeed Moghaddam
Department of Mechanical and Aerospace Engineering,
University of Florida,
Gainesville, FL 32611
e-mail: saeedmog@ufl.edu

In this study, six benchmark experiments are conducted on bubbles at different growth stages to evaluate the assumptions of the existing microchannel flow boiling heat transfer models/hypothesis. The results show that the bubble ebullition process triggers a spike in the local surface heat flux due to the thin film evaporation and transient conduction heat transfer mechanisms. This enhancement in the surface heat flux is limited to a very small area at the bubble–surface contact region at the nucleation site limiting the overall heat transfer contribution of the bubble ebullition process. The contribution of these two mechanisms of heat transfer increases as the bubble–surface contact area becomes larger. As the bubbles length increases, the time period of activation of the microlayer evaporation mechanism substantially increases while that of the transient conduction mechanism remains relatively unchanged. When the microchannel is mostly occupied by bubbles, the thin film evaporation mechanism becomes the dominant heat transfer mode. The results clearly indicate that single-phase heat transfer mechanism active at surface regions not covered by bubbles is governed by the laminar flow theory (for the test conditions presented here). In essence, a measureable enhancement effect in the liquid phase due to bubbles growth and flow has not been observed. A comparison with the existing microchannel flow boiling models suggests that the three-zone flow boiling model can qualitatively describe the heat transfer events observed in this experiment but fails to accurately predict the magnitude of the heat transfer mechanisms.
[DOI: 10.1115/1.4036655]

1 Introduction

The flow boiling process is an efficient mechanism of heat transfer that has enabled a set of key technologies such as boilers and evaporators over the past several decades. A high heat transfer coefficient, low mass flux, and nearly constant streamwise temperature are the main attributes of the flow boiling process that has made its use attractive in traditional applications. Similar reasons have motivated the scientific community to extend the use of the flow boiling process in microchannels [1–10] for thermal management of modern miniaturized energy devices, high-power electronics, solid-state lasers, etc. To do so, numerous studies have been conducted for more than a decade to understand the physics of heat transfer in the microchannel flow boiling process. The understanding of the process physics is the key to development of high-performance microchannel heat sinks and modeling/predictive tools. The existing microchannel flow boiling models are limited and are based on hypotheses that are often contradictory and have not been experimentally verified due to the lack of adequate experimental tools.

Jakob [11] was among the first to attempt rationalizing the enhanced heat transfer effect observed in the boiling process. He postulated that the enhanced heat transfer associated with the saturated pool boiling process is due to liquid agitation at the wake of bubbles departing from the surface. This mechanism of enhancement was later named the "microconvection" mechanism. To formulate heat transfer through this mechanism, analytical expressions for bubble radii and growth rates were utilized to define a Reynolds number representative of the induced convective effect in the superheated liquid layer adjacent to the heated wall. This interpretation of the pool boiling heat transfer process was then borrowed by Rohsenow [12] and subsequently by Chen [13] to explain the flow boiling heat transfer process in tubes. Rohsenow [12] suggested that heat transfer during the flow boiling process consists of two basic mechanisms: the macroconvective mechanism due to the bulk motion of the fluid and the microconvective mechanism associated with the nucleate boiling process. He further hypothesized that the forced convective and nucleate boiling mechanisms are additive in their contribution to the overall surface heat transfer [12]. Although the microconvection hypothesis was never independently verified, the superimposed concept has since been utilized by many researchers to correlate flow boiling in conventional-sized channels (i.e., macrochannels) [2,13–16]. A more recent study by Moghaddam and Kiger [17] suggests that the enhanced convective effect generated at the wake of a bubble is not the only mechanism of heat transfer at the nucleation site. Their studies suggested that the microlayer evaporation and transient conduction mechanisms play a substantial role in the overall heat transfer at the nucleation site. However, the relative contribution of the three mechanisms (microconvection, thin film evaporation, and transient conduction) depends on the surface superheat and the nucleation site density as well as the liquid properties. Perhaps, since heat transfer through these mechanisms is also related to the bubble diameter and its growth rate, surface superheat, and liquid properties (i.e., parameters used in Jakob's [11] model), their effect could have been captured by the empirical coefficients incorporated into the model.

The introduction of microchannels in the late 20th century further complicated the flow boiling modeling task. This complication arises from the physics of scale; due to the fact that when the channel size is reduced to that of the bubble, as will be shown later, the heat transfer processes triggered by the bubble growth and flow process vastly change at different stages of bubble growth. Furthermore, the confinement effect and changes in balance of forces greatly impacts the flow dynamics and consequently the role and relative contributions of different heat

Contributed by the Heat Transfer Division of ASME for publication in the JOURNAL OF HEAT TRANSFER. Manuscript received September 21, 2016; final manuscript received February 23, 2017; published online June 21, 2017. Assoc. Editor: Peter Stephan.

transfer mechanisms. Hence, inaccuracy of assumptions made with regards to the role of bubbles on the surface heat transfer enhancement can greatly impact the accuracy of the models.

To understand the physics governing the heat transfer process in microchannels, numerous studies have been conducted and several models have been developed [18–22]. The developed models are fundamentally different in their assumptions of the process physics. The first set of models introduced here are those [16,18,19] developed based on the superimposed concept originally presented for macrochannels, as mentioned earlier. The fundamental assumption of this model is that convection (both micro-and macroconvection) is the primary mode of heat transfer in microchannels. Considering that most microchannel flows are laminar [2], attempts have been made [18] to use laminar single-phase heat transfer coefficient for the convective term.

The second hypothesis implemented to explain heat transfer in the microchannel flow boiling process assumes that direct evaporation of thin liquid films is the dominant mechanism of heat transfer in microchannels. The annular two-phase flow model of Qu and Mudawar [21] and three-zone model of Thome et al. [22] are the prominent microchannel flow boiling models developed based on the thin film evaporation mechanism. Qu and Mudawar [21] assumed that the dominant flow pattern in microchannels is the annular flow regime. This model assumes that the microchannel flow consists of a thin liquid film flowing on the channel wall along with a continuous vapor core at the center of the channel. It is also considered that the vapor core contains entrained droplets. The liquid film thickness is assumed to be uniform along the channel and small compared to the channel hydraulic diameter. Mass transfer between the liquid film and the vapor core occurs at the liquid–vapor interface along the flow direction. This model assumes that the evaporation of the liquid film is the main heat transfer mechanism in microchannel. Mass flow rate of the liquid film and its thickness, axial pressure gradient, and interfacial shear stress are four primary parameters of the model. Other thermohydraulic parameters including the heat transfer coefficient are evaluated using the primary parameters.

The three-zone flow boiling model of Thome et al. [22] assumes that the heat transfer events in the flow boiling process are cyclic and strongly depend on the bubble frequency and thickness of the liquid film formed on the channel wall. The three-zone model suggests that heat transfer associated with the thin film evaporation process is typically several times that of the liquid slug [22]. Thome et al. [22] assumed that bubbles nucleate and quickly grow in a uniformly superheated liquid to the internal diameter of the microchannel before departure from the nucleation site. Each bubble was envisioned as a "shutter" that divides the liquid flow into successive liquid slugs. A growing bubble was assumed to trap a thin liquid film on the flow channel wall. The thickness of the liquid film plays an important role in the surface heat transfer. At a fixed location, Thome et al. [22] explained the process as follows: (i) a liquid slug passes, (ii) an elongated bubble passes, and (iii) if the liquid film trapped underneath the bubble dries out before arrival of the next liquid slug, a vapor slug passes. The cycle then repeats itself upon arrival of the next liquid slug. The model predicts the local heat transfer coefficient at a fixed location along a microchannel subjected to a uniform heat flux boundary condition.

Performance of these models has often been assessed by their ability to predict the overall surface heat transfer coefficient, which is the cumulative effect of boiling heat transfer subprocesses. Evidently, the first step in advancing the microchannel flow boiling modeling is to decipher the physics of the process through experimental analysis of the microscale heat transfer events. In this study, we used a unique measurement approach comprehensively described in our previous publications [4,23] to conduct six benchmark experiments and examine current hypotheses about the microchannel flow boiling process. The first three experiments summarize key findings of our prior publications. The other three experiments provide new insights on the nature of microscale phase change heat transfer events associated with a nucleating and departing bubble, successive bubbles generated at different frequencies, and a long liquid slug trapped between two consecutive vapor slugs. In Secs. 2–4, first, the measurement approach and experimental setup are briefly presented. Then, the benchmark experiments and their results are discussed. Finally, the findings are compared against the fundamental hypotheses of the microchannel flow boiling models discussed earlier in this section.

2 Test Article

Measurement of the surface heat flux is the key challenge in resolving the thermal field at the surface–liquid interface at a sufficiently high spatial and temporal resolution. The local heat flux at the solid–fluid interface rapidly varies in time and space as a result of changes in boundary conditions due to bubbles nucleation, expansion, and flow along the channel. Most previous measurement techniques rely on utilizing a monolithic material as the test substrate. The primary issue associated with these techniques is evinced by presence of a significant heat flow within the solid substrate coupling boiling subprocesses as it has been shown by the experimental results of Yabuki and Nakabeppu [24] and Rao et al. [25]. This coupling between the heat transfer events does not allow to study (and model) the individual boiling subprocesses separately and determine their role on the overall surface heat transfer [4]. The measurement approach utilized in this study overcomes shortcomings inherent to using a monolithic substrate as it has been comprehensively discussed in our previous publications [4,17,23,26].

A detailed view of the test article is shown in Fig. 1. The test article has a composite substrate that consists of a relatively thick high thermal conductivity (high-k) material (i.e., 500-μm thick Si with a thermal conductivity of 130 W m^{-1} K^{-1}) coated by a relatively thin layer of a low thermal conductivity (low-k) polymer (i.e., 9.8-μm thick SU8 with a thermal conductivity of 0.2 W m^{-1} K^{-1}). Two separate arrays of platinum-based resistance temperature detectors (RTD) are embedded within the composite wall to record temperature variations at the Si–SU8 and SU8–fluid

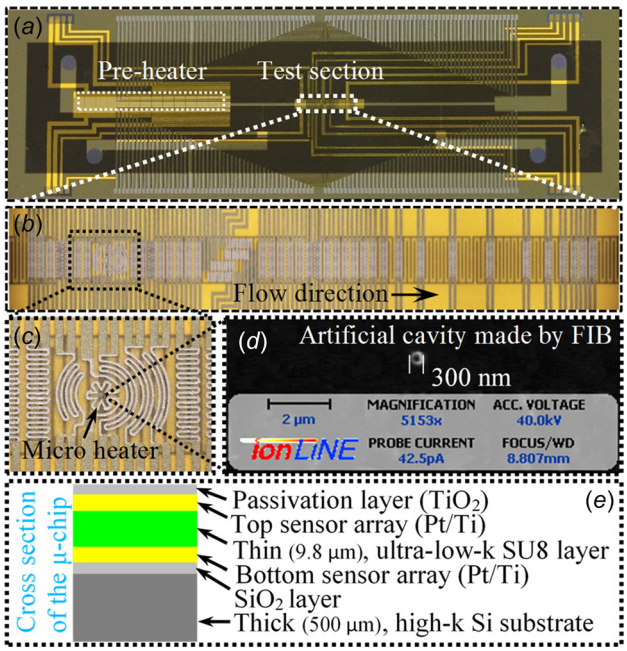

Fig. 1 (*a*) An image of the microfluidic chip (preheater and test sections are labeled), (*b*) a close view of the test section, (*c*) a zoomed view of the pulsed function microheater, (*d*) an SEM image of the artificial cavity, and (*e*) a schematic view of the composite substrate cross section

interfaces. Several thin film heaters are also embedded at the Si–SU8 interface. In the boiling experiments of dielectric liquids (e.g., FC-72), the surface temperature at the Si–SU8 interface remains at a relatively constant temperature owning to the high thermal conductivity of the Si substrate. Any change in the surface heat flux directly changes the temperature at the top of the polymer layer. The thermal field within the SU8 layer is then numerically solved to determine the surface heat flux at the SU8–fluid interface using the measured temperature boundary conditions on both sides of the SU8 layer [4,23].

A single rectangular microchannel is built on the substrate with inlet and outlet ports for fluid entry and exit. The microchannel wall is made of a 75-μm thick SU8 film and is sealed by a polydimethylsiloxane (PDMS) transparent cap. The microchannel width is 300 μm. An on-chip preheater heats up the test fluid to the desired temperature before entering the test section. To fix the nucleation site, a 300 nm in diameter dedicated cavity is fabricated after the preheater using a focused ion beam (FIB) milling machine. The cavity is surrounded by a pulsed function microheater (cf. Fig. 1(*c*)). Changing the amplitude and period of the excitation voltage applied to the microheater subjects the liquid region immediately adjacent to the cavity to different metastable superheated conditions (i.e., nonequilibrium thermodynamic conditions) [27]. As a result, the liquid undergoes phase change generating different flow regimes. Since the total surface covered by the microheater is quite small ($\sim$0.004 mm^2), the heat supplied to the liquid is negligible.

3 Experimental Apparatus, Uncertainty Analysis, and Single-Phase Calibration Tests

An experimental test facility was fabricated to conduct the microchannel flow boiling experiments. A four-wire configuration, also referred to as a Kelvin connection, is utilized to increase the temperature measurement accuracy. The four-wire configuration uses one pair of wires to deliver the excitation current (Ex. $\pm$) to the RTD sensor and uses a separate pair of wires to sense the voltage across the sensor (Ch. $\pm$). Because of the high input impedance of the differential amplifier, negligible current flows through the sense wires. This results in a negligible voltage drop error due to the lead resistance [28]. The microfluidic chip is then wire bonded to a custom-made double-sided printed circuit board (PCB) before connecting to a high-speed data acquisition (DAQ) system. The DAQ system which consists of a current excitation module (NI SCXI-1581), a channel amplifier module (i.e., signal conditioning module) (NI SCXI-1120C), a high-speed DAQ module (NI PXI-6289), and a programmable DC power supply module (NI PXI-4110) is commanded by an embedded controller (NI PXI-8115). The temperature data and the synchronized bubble images captured by a high-speed camera (FASTCAM SA4-Photron) are recorded at a frequency of 20 kHz. In addition, the pulsed function microheater is connected to the programmable DC power supply module. Data collections as well as controlling the applied dc voltage to the pulsed function microheater are performed using a LABVIEW program. The thin film heaters are also powered by the NI PXI-4110 dc power supply.

The working fluid is delivered to the microfluidic chip by a piezoelectric micropump (Model MP6, manufactured by Bartels Mikrotechnik GmbH, Dortmund, Germany). Two PX-26 pressure transducers with $\pm$1% reading error are used to measure the pressure drop across the microchannel. The working fluid is degassed by vigorous boiling for several hours before each experiment. Then, the desired surface temperature is adjusted and allowed about 15 min to reach steady state before recording the data. The steady-state condition is rapidly achieved due to the small mass of the test section.

The RTD sensors are calibrated prior to the flow boiling experiments to obtain the voltage–temperature relationship of each sensor. The calibration tests are done in a uniform temperature oven for a temperature range of 40–90 °C. A constant current excitation of 100 μA is supplied to each sensor. Temperature sensors have a negligible self-heating. The obtained voltage–temperature (V–T) curves show a linear trend and the sensitivity of the RTD sensors (the slope of the V–T curves) is 0.13 mV/°C. The data acquisition system has a maximum uncertainty of $\pm$28 μV at a gain of 100 with a minimum detectable voltage change of 1 μV. Considering the sensitivity of the sensors and the voltage uncertainty, the maximum temperature measurement error is determined to be $\pm$0.25 °C. In addition, the maximum uncertainty in measurement of the SU8 film thickness and the local heat flux data are $\pm$0.01 μm and $\pm$1 W/cm^2, respectively.

In addition, single-phase flow tests at different mass flow rates and heat fluxes are conducted to verify that the current experimental setup is able to satisfactorily measure the heat transfer coefficient. Since the reciprocal of the Graetz number, $\mathrm{Gz}^{-1} = x/(D\ \mathrm{Re_D}\ \mathrm{Pr})$, is more than 1.5, the flow is fully developed at the test section (cf. Fig. 2). The Nusselt number (Nu) for fully developed laminar flow in a rectangular channel with one side heated and one side insulated at a constant heat flux is 5.39 [1]. Prior to the single-phase flow test, the device heat loss to the ambient is measured as a function of its surface temperature at a dry state. The energy supplied to the device to maintain it at a set temperature is considered to be its heat loss. The tests are conducted at mass fluxes of 68.4 kg/m^2 s (Re = 12.8) and 93.3 kg/m^2 s (Re = 17.5) at heat fluxes of 1 and 1.3 W/cm^2, respectively.

Figure 3 provides the experimental Nu values at sensor locations S1, S2, and S3 (cf. Fig. 2) and their comparison with the analytical values. The reciprocal of the Graetz number for sensors S1, S2, and S3 are 2.92, 3.31, and 3.62, respectively. The experimental values are determined using the average surface heat flux and temperature; a commonly practiced method. However, recognizing that the surface heat flux and temperature cannot be constant simultaneously, a more realistic approach is to conduct a single-phase numerical simulation employing experimentally measured temperature values at the solid–fluid interface. The fully developed Nu number calculated with this method is also shown in Fig. 3. As it can be seen, there is a good overall agreement between the experimental, analytical, and numerical Nusselt numbers (the difference between the three is within the experimental uncertainty).

4 Results and Discussion

The schematic of Fig. 4 depicts various stages of bubbles growth and flow in a microchannel. After nucleation and departure, the bubble grows into a vapor slug that continues to expand along the channel length. When the length of the vapor slug substantially increases, the thin liquid film around it fully evaporates leading to the surface partial dryout. To resolve the heat transfer events associated with the flow dynamics, a comprehensive set of tests was presented. In Secs. 4.1–4.8, first, six benchmark experiments including three reviews and three new tests are provided to analyze the surface thermal response associated with different stages of bubble growth. Then, the results of the experimental findings are utilized to critically assess the existing microchannel flow boiling heat transfer theories.

4.1 Long Vapor Slug. The first benchmark experiment comprehensively explained in Ref. [4] elucidates heat transfer events of a long vapor slug during its growth in the microchannel. The test was conducted at a mass flux of 68.4 kg/m^2 s. Figure 5(*a*) shows the sequential images of the vapor slug. The corresponding temperature data at an arbitrarily chosen sensor (S26) at the Si–SU8 and SU8–fluid interfaces are shown in Fig. 5(*b*). An arbitrary time before the arrival of the vapor slug at the sensor is chosen as the time reference. The bubble passing time (τ) over the sensor is 14 ms. As the results suggest, the Si–SU8 interface temperature remains at a relatively constant temperature of 66 °C, while the SU8–fluid interface temperature rapidly varies in response to changes in the fluid side boundary conditions. The heat flux data are provided in Fig. 5(*c*).

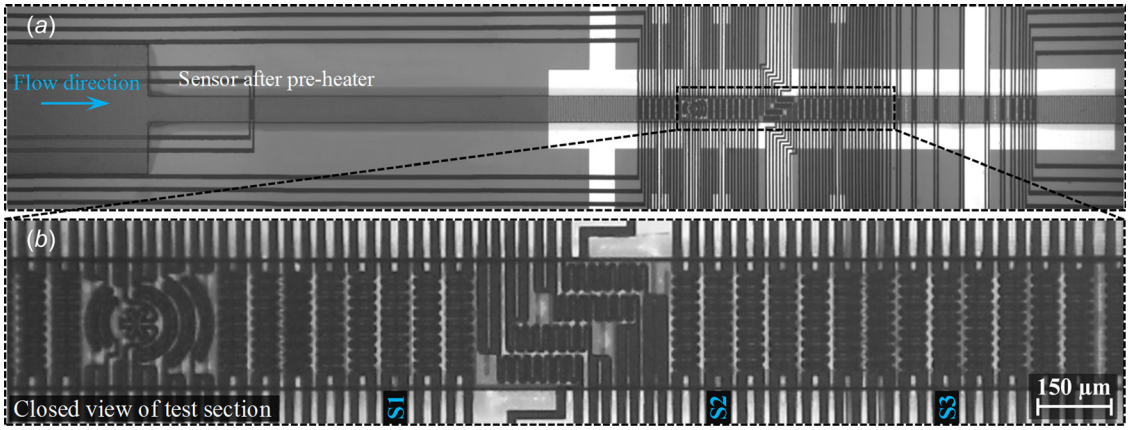

Fig. 2 (*a*) A zoomed out view of the microchannel and (*b*) a close view of the test section and the sensors chosen for the single-phase flow tests

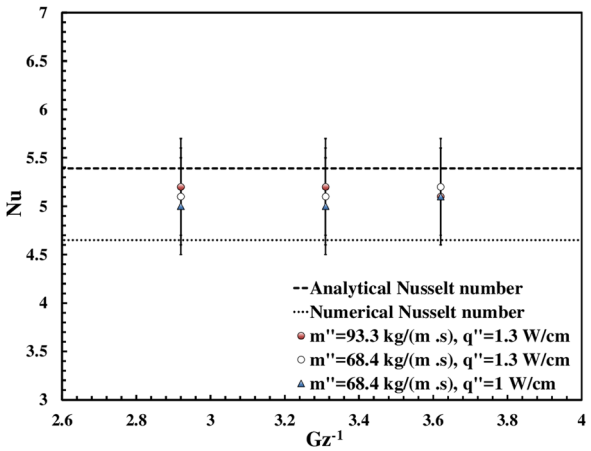

Fig. 3 Comparison of the experimental, theoretical, and numerical Nusselt values

Comparison of the bubble images with the synchronized temperature data suggests that the surface temperature is relatively constant before the arrival of the vapor slug at sensor S26 at $t = 1$ ms. Upon the arrival of the vapor slug at the sensor, a rapid decline in temperature is recorded. This decline in the surface temperature is due to the microlayer and interline evaporation modes of heat transfer associated with the evaporation of a thin liquid film formed between the solid surface and the vapor slug. Figure 5(*c*) depicts the heat flux spike associated with this thermal event. After a while (during $t \approx 6$–9 ms), the surface heat flux associated with this mechanism of heat transfer starts to decline due to the dryout of the thin liquid film left on the sensor. However, the surface heat flux does not immediately reach to zero and instead enters a new phase (from $t \approx 9$ to 15 ms) during which it gradually declines. This decreasing trend in the local heat flux can be explained by examining the bubble images (cf. comparison of images C and D in Fig. 5(*a*)), where it can be observed that the liquid layers trapped at the two sides of the vapor slug gradually disappear due to evaporation. This evaporating mass of liquid that covers edges of the sensor sustains a low and gradually declining surface heat flux. A careful delineation of different elements of these events involving analysis of the thermal field at other sensors as well as a test conducted in another conditions is provided in Bigham and Moghaddam (Sec. 6-1) [4].

Comparison of the temperature data with the bubble images also reveals that the surface undergoes a second rapid decline in temperature as the rear end of the vapor slug rewets the sensor footprint, suggesting a second rapid cooling event (cf. Fig. 5(*c*)). This sudden spike in the local heat flux during the rewetting process resembles the observations made in pool boiling studies [17,29] during the bubble departure, as a liquid front advances over (i.e., rewets) the bubble-surface contact area after a dryout period following the microlayer evaporation process. This phenomenon arises from a mismatch between the surface and liquid temperatures as they come into contact. The physics of this process is consistent with what is commonly named as "transient conduction" mode of heat transfer that results from the rewetting of a hot surface with the cooler bulk liquid. At the end of this process, when liquid fully rewets the sensor, the local heat flux gradually declines and reaches to that of a single-phase convection process. The heat flux through this mechanism remains nearly constant for short liquid slugs (the variations are within the experimental uncertainty). However, as it will be shown later, the surface heat flux associated with long liquid slugs slowly declines as the liquid temperature approaches the surface temperature.

4.2 Short Vapor Slug. The second benchmark experiment extensively described in Ref. [23] reveals the surface heat transfer events associated with the flow of a short vapor slug. Figure 6 shows the images of the vapor slug along with the corresponding temperature and heat flux data at sensor S18. The slug passing time over the sensor (τ) is 5.3 ms. The average temperature at the Si–SU8 interface is kept at 66 °C. Overall, the observed thermal trends are similar to those of the first benchmark study. As expected, the surface temperature drops due to a spike in the local heat flux when the front side of the slug arrives at the sensor footprint. This is an indicative of microlayer and interline evaporation modes of heat transfer. However, in contrast to the case of a long vapor slug, the rear end of the slug arrives at the sensor footprint before the microlayer fully evaporates, resulting in truncation of

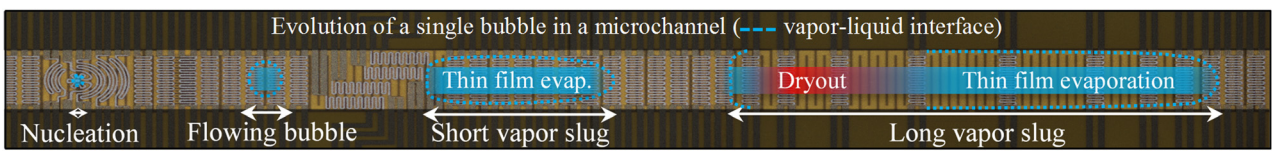

Fig. 4 A schematic representation of different stages of bubble growth in a microchannel

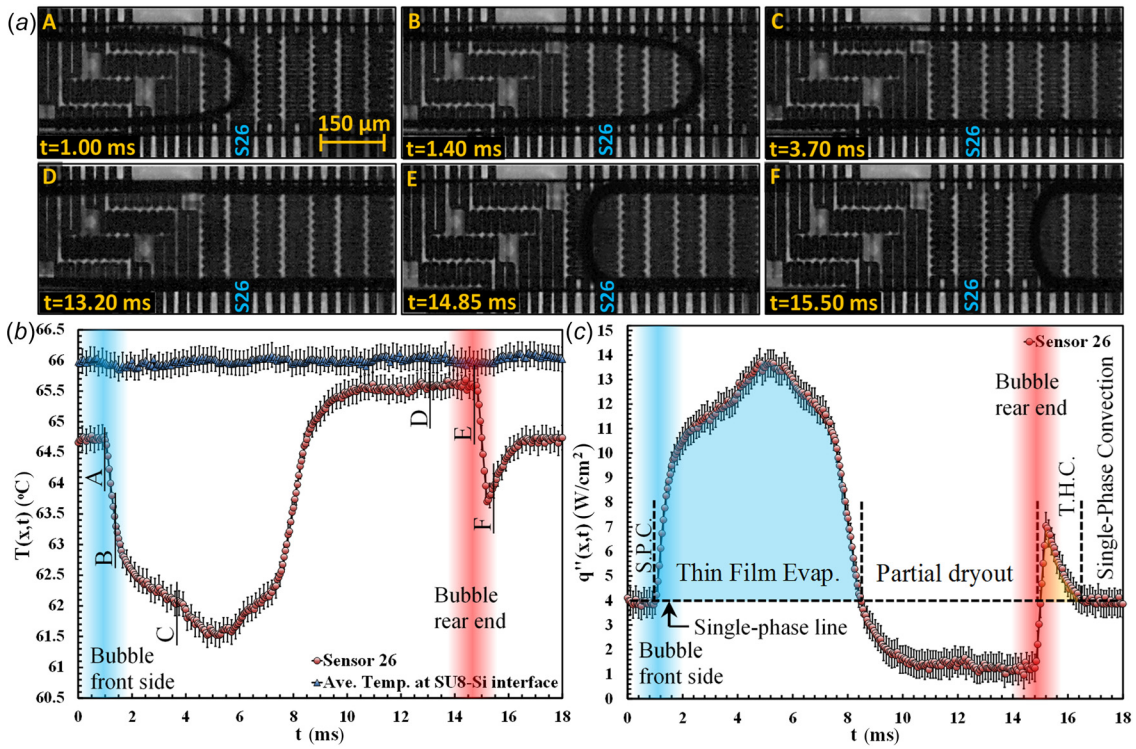

Fig. 5 (*a*) Images of a long vapor slug, (*b*) surface temperature history, and (*c*) respective local heat flux data. Test is conducted at a mass flux of 68.4 kg/m^2 s (average temperature at the SU8–Si interface and vapor slug passing time over the sensor are 66 °C and 14 ms, respectively).

the thin film evaporation heat transfer event. Consequently, the thin film evaporation and the transient conduction heat transfer events appear as a single heat flux peak.

4.3 Flowing Bubble. The third benchmark experiment explained in more details in Ref. [23] provides the local thermal field associated with a bubble that is not fully confided by the microchannel walls. Figure 7 shows the images and the corresponding temperature and heat flux data of a bubble at sensor S14. Compared to the tests discussed in Secs. 4.1 and 4.2, the bubble passing time over the sensor is significantly short, $\tau = 1.4$ ms. As a result, the microlayer evaporation heat transfer event is truncated quite early resulting in a significant decline in the surface heat flux.

4.4 Nucleating and Departing Bubble. The fourth benchmark experiment describes heat transfer events during nucleate boiling process. Figure 8 shows images of a bubble during its nucleation, growth, and departure steps. The bubble is evolved from the nanoscale artificial cavity. In this test, the star-shape thin film pulsed function microheater is utilized as a RTD sensor. The departure time is defined as the moment the bubble moves away from the center of the star-shape sensor. Figure 9(*a*) shows the corresponding surface temperature of the sensor as well as the average temperature of the sensors embedded at the Si–SU8 interface. As it can be seen, the temperature at the Si–SU8 interface is almost constant, within the 64.7–64.9 °C range. Comparison of the bubble images with the temperature data indicates that the surface temperature continuously declines during the bubble formation and growth. The observed temperature drop is due to the microlayer/interline evaporation modes of heat transfer. Figure 9(*c*) presents the bubble growth rate as a function of time. At $t \approx 0.75$ ms, the bubble departs from the nucleation site and the contact line passes over the center of the sensor. The bubble diameter at departure is $\sim 110\ \mu$m (cf. images D and E in Fig. 8). After the bubble departure, the surface temperature starts increasing. Once the bubble completely passes over the sensor, the surface temperature recovers to that of the single-phase flow condition. Figure 9(*b*) shows the corresponding surface heat flux. As expected from the temperature data, the surface heat flux spikes as the bubble nucleates and grows over the sensor. This is due to microlayer/interline evaporation mode of heat transfer at the bubble–surface interface. Once the bubble departs from its nucleation site, the surface heat flux gradually decreases and reaches to a steady-state condition.

4.5 Successive Bubbles. The benchmark experiments discussed in Secs. 4.1–4.4 were conducted at the isolated bubble regime in which the flow dynamics and the wall thermal field associated with a bubble are not impacted by a preceding bubble. This is the case below a certain bubble generation frequency (i.e., approximately 100 bubbles per second for the mass flux tested here), as clearly illustrated in Fig. 10, which provides local heat flux-time history of two subsequent bubbles at a bubble generation frequency of 56 bubbles/s. The surface heat transfer signatures associated with successive bubbles are temporally segregated. However, increasing the bubble generation frequency can change the surface thermal events substantially. This condition is elucidated in Fig. 11, which shows the heat transfer events associated with successive moving bubbles at a bubble generation rate of approximately 190 bubbles/s. As the results indicate, the thin film evaporation mode of heat transfer starts when the first vapor slug (V.S.1) arrives at sensor S26 (cf. Fig. 11(*a*) and corresponding heat flux data in Fig. 11(*e*)). V.S.1 leaves S26 at $t = 5.9$ ms and the heat flux consequently drops. However, the second vapor slug (V.S.2) arrives at the sensor at $t = 7.35$ ms before the transient heat conduction event associated with V.S.1 ends, resulting in an increase in the heat flux due to the thin film evaporation mechanism (cf. Fig. 11(*c*)). The results show that the single-phase convection heat transfer mode is circumvented at a high bubble generation frequency.

4.6 Long Liquid Slug. In contrast to the previous case, the surface thermal field can substantially change, and single-phase

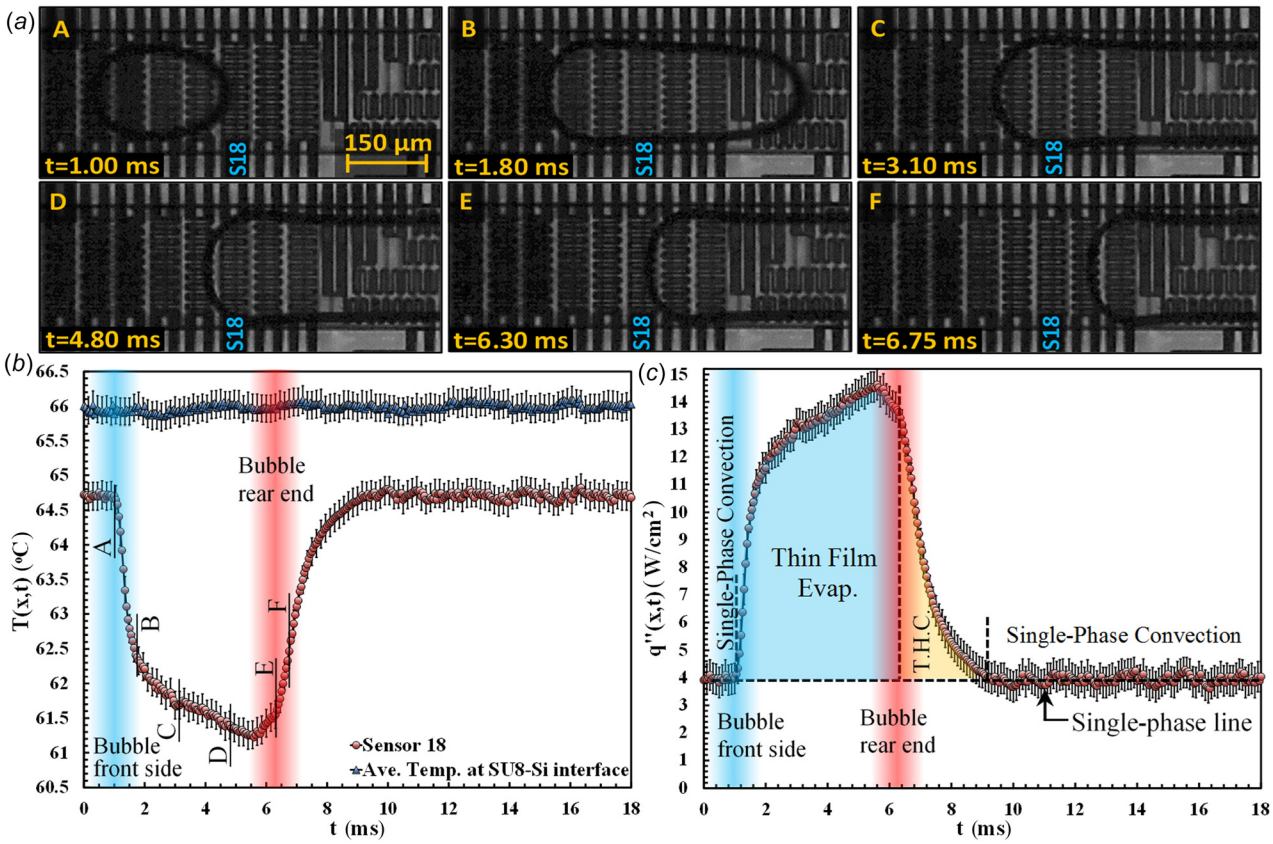

Fig. 6 (*a*) Images of a short vapor slug (average temperature at SU8–Si interface and vapor slug passing time over the sensor are 66 °C and 5.3 ms, respectively), (*b*) surface temperature history, and (*c*) respective local heat flux data

convection can become the primary mode of heat transfer, if bubbles are generated at a substantially lower frequency. To better understand the heat transfer nature to a long liquid slug associated with a low bubble frequency regime, an experiment was conducted at a bubble generation rate of ~12 bubbles/s. The results (cf. Fig. 12) show that the single-phase heat flux (after $t \approx 10$ ms) gradually declines. This trend is consistent with the single-phase duct flow theory, as we expect the surface heat flux

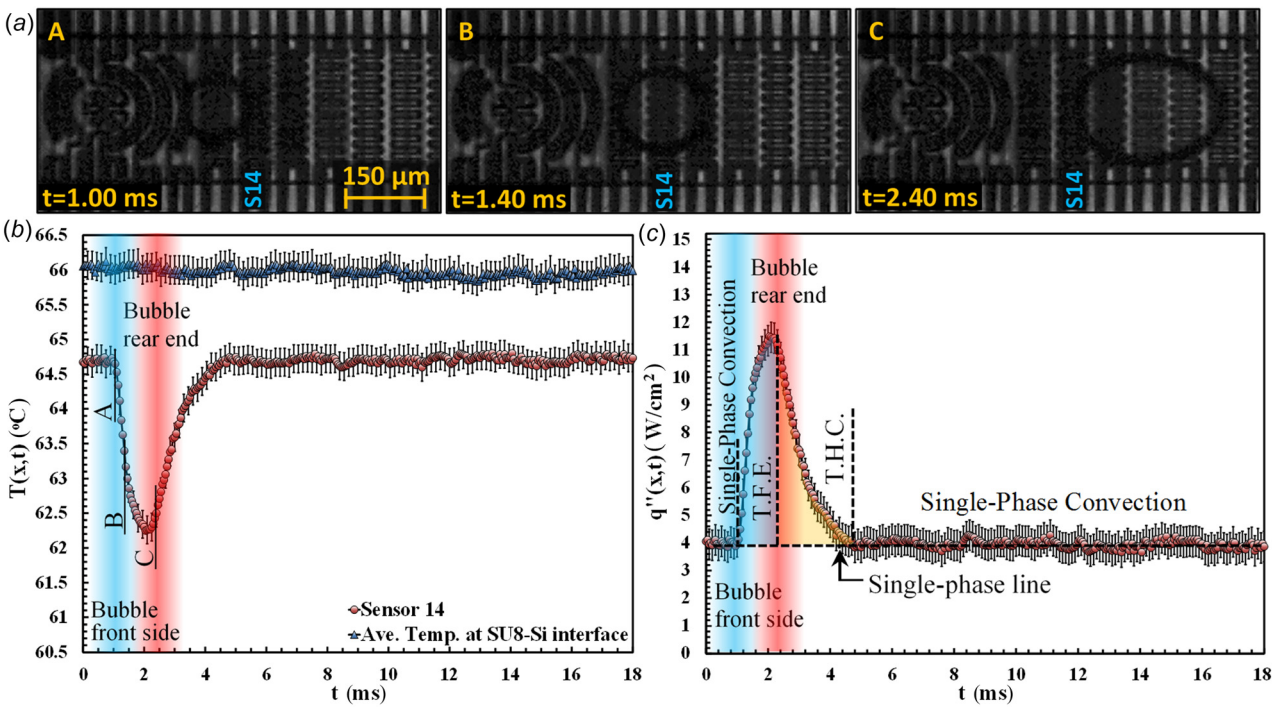

Fig. 7 (*a*) Images, (*b*) surface temperature history, and (*c*) local heat flux data corresponding to a bubble with a passing time of 1.4 ms. Test is conducted at a mass flux of 68.4 kg/m^2 s (average temperature at the SU8–Si interface is 66 °C).

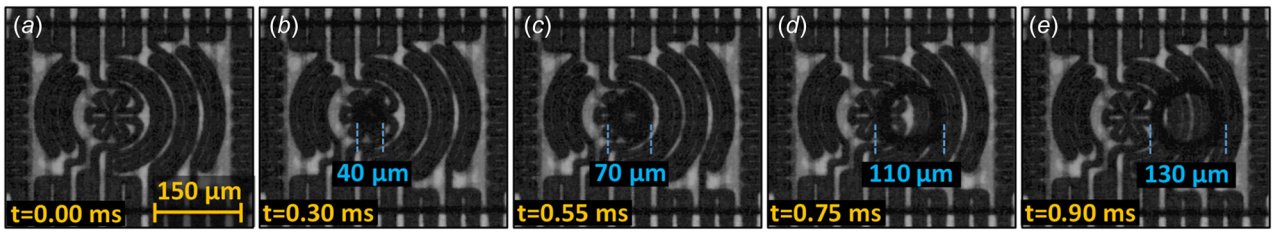

Fig. 8 Images of a nucleating bubble in microchannel flow boiling process (average temperature at the SU8–Si interface is 64.8 °C)

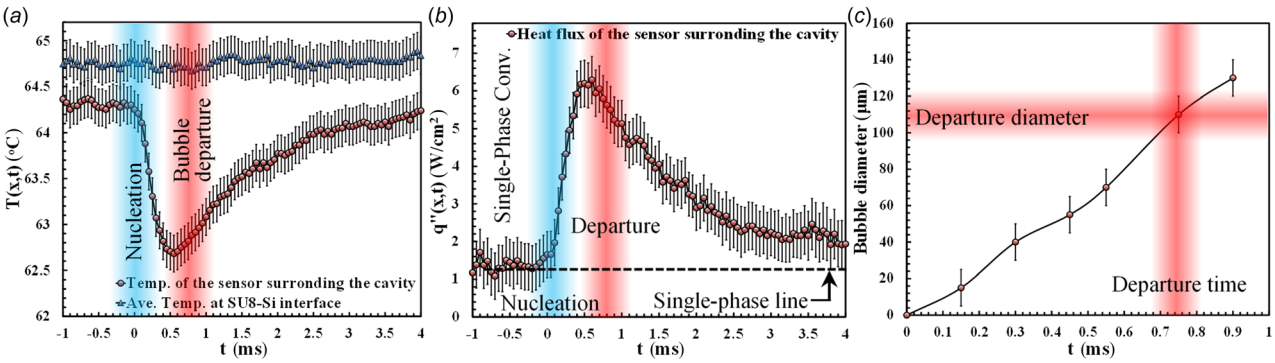

Fig. 9 (*a*) Surface temperature history associated with a nucleating bubble shown in Fig. 8 (average temperature at the SU8–Si interface is 68.4 °C), (*b*) respective local heat flux data, and (*c*) bubble growth and departure as a function of time

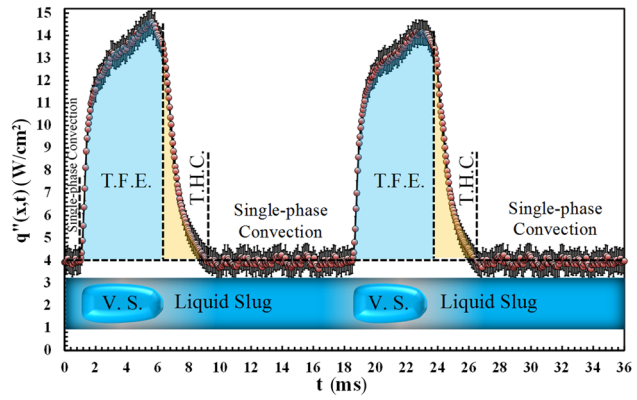

Fig. 10 Local heat flux history of two subsequent bubbles at a bubble generation frequency of 56 bubbles/s

to decline under a constant surface temperature boundary condition, since the liquid temperature approaches the surface temperature. In this case, the liquid has substantially warmed up prior to moving over sensor S19. It must be highlighted that the length of this liquid slug, and hence, its heating time is an order of magnitude longer than the liquid slugs observed in tests discussed in Secs. 4.1–4.5.

4.7 Detailed Breakdown and Relative Contributions of Different Heat Transfer Mechanisms. Experimental results presented in Secs. 4.1–4.6 suggest that the microchannel flow boiling heat transfer process consists of several basic heat transfer mechanisms. Contributions of these mechanisms to the overall surface heat transfer depend on the activation time period of each mechanism. Table 1 provides a detailed breakdown of the magnitude of all heat transfer mechanisms and their relative contributions, as a function of the bubble passing time at a bubble generation frequency of 56 bubbles/s. The values presented for the bubble passing times over a sensor (τ) correspond to different sensors

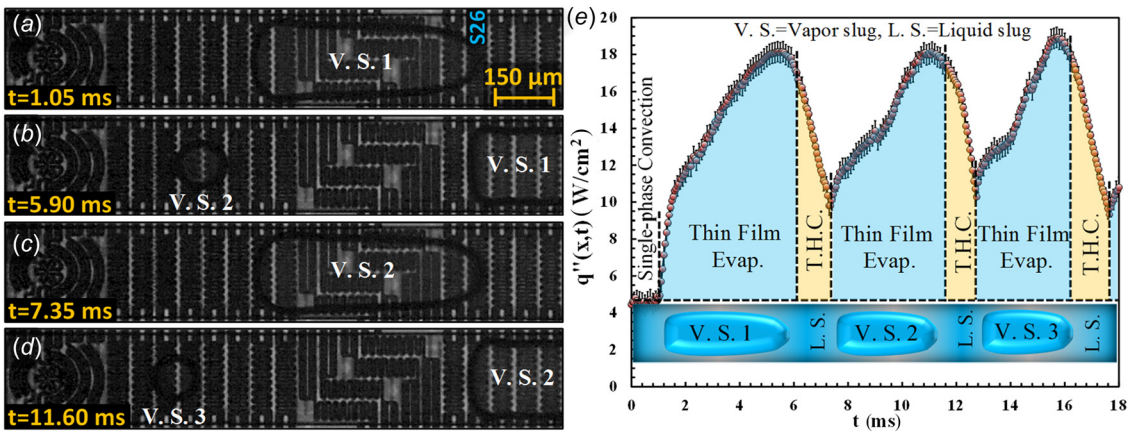

Fig. 11 (*a*)–(*d*) Images and (*e*) local heat flux history corresponding to successive moving bubbles at a bubble generation rate of approximately 190 bubbles/s and a mass flux of 93.3 kg/m^2 s

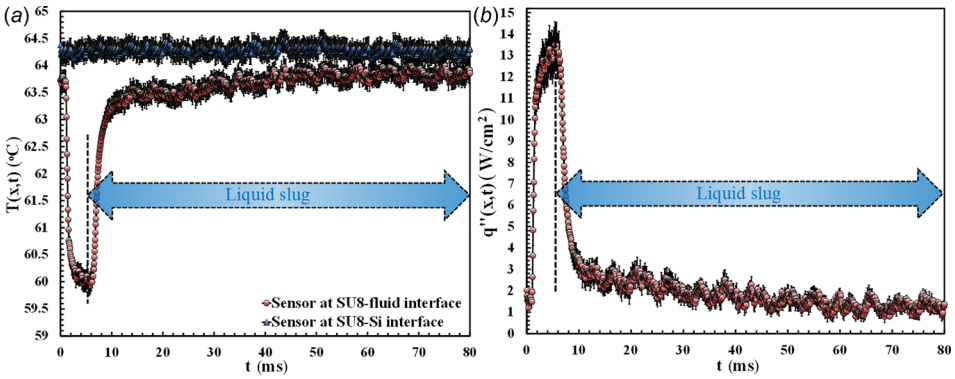

Fig. 12 (*a*) Surface temperature history and (*b*) heat flux data corresponding to a long liquid slug at a bubble generation frequency of ~12 bubbles/s. Test is conducted at a mass flux of 93.3 kg/m^2 s (average temperature at the SU8–Si interface is 64.2 °C).

positioned along the flow direction. For a sensor at the upstream (i.e., a bubble passing time of 1.4 ms), it can be seen that the contribution of the thin film evaporation, the most effective heat transfer mode, is small due to a short bubble passing time. The single-phase convection heat transfer mode, the least effective heat transfer mechanism, is active for a longer time period. As the bubble passing time over a sensor increases, the contribution of the thin film evaporation mechanism increases while that of the single-phase convection declines. The total heat transfer reaches its maximum value at a bubble passing time of 5.3 ms. Beyond this passing time period, a partial dryout leads to a decline in the overall surface heat transfer.

4.8 Comparison With the Existing Hypothesis. As mentioned in the Introduction section, two main theories developed to model microchannel flow boiling heat transfer are based on the superposition concept and the thin film evaporation mechanism. Models based on the superposition concept assume that the role of nucleate boiling in enhancing the surface heat transfer in microchannels and pool boiling is similar. To shed light on the main differences between the two, here we provide a brief summary of the findings of Moghaddam and Kiger [17] on the role of nucleation on surface heat transfer enhancement in pool boiling. In their experiments, vapor bubbles were generated from an artificial nucleation site surrounded by 44 radially distributed sensors. Figure 13 shows the images of a bubble during nucleation, growth, and departure in pool boiling of FC-72. The corresponding surface heat flux values are provided in Fig. 14. A comparison of the bubble images and the temperature data shows that formation of a bubble results in a spike in surface heat flux due to microlayer/interline evaporation. These spikes start at the center of the array (i.e., at sensor S-1) and progress over the subsequent sensors (i.e., sensors S-2 to S-8). The durations of these spikes are on the order of 1 ms and correspond to the microlayer evaporation time. It can be seen that the local heat fluxes start to decrease shortly after the initial rise indicating that the microlayer is mostly evaporated. The heat flux data show a second phase of rise in heat flux after the bubble–surface contact area reaches its maximum diameter and the advancing liquid rewets the dried bubble–surface contact area. This transient mechanism of heat transfer results from the rewetting of the superheated wall with cooler bulk liquid, the so-called transient conduction mode that was described in Secs. 4.1 and 4.2. Moghaddam and Kiger's tests [17] further suggested that the bubbling events generate an almost constant enhanced convective effect around the bubble–surface contact area, which can be identified as the microconvection heat transfer mechanism hypothesized in early boiling models [17,26,30,31]. Unlike the microlayer and transient conduction mechanisms, this process had a steady nature in all test conditions.

Although a study with such level of details has not been conducted in the macrochannel flow boiling process, all three mechanisms of heat transfer discussed previously can conceivably be active in the flow boiling process, albeit with different contribution levels. In the flow boiling process, the drag force applied on a growing bubble results in early bubble departure with a substantially smaller bubble–surface contact area and associated heat transfer mechanisms. Our microchannel test results clearly show that nucleation does not trigger microconvective effects (no enhancement in single-phase convection heat transfer is observed). Hence, care needs to be taken when extending the Jakob's [11] hypothesis to microchannels. Under the test conditions of this study, the viscous forces dominate the flow regime (i.e., Re = 12.8) and do not allow effective agitation of the liquid at the vicinity of the surface.

Microchannel flow boiling models based on the thin film evaporation mechanism consider thin film evaporation as the dominant heat transfer mode. Our experimental results also imply that thin film evaporation is the most effective mechanism among various heat transfer mechanisms. As mentioned earlier, the two prominent thin film models are the annular two-phase flow model of Qu and Mudawar [21] and the three-zone model of Thome et al. [22]. The annular two-phase flow model of Qu and Mudawar [21] presumes that a steady annular flow is always present in the microchannel. This assumption is in contrast with the experimental observations of the present study. As it has been shown in Fig. 5(*c*), the thin liquid film disappears within 6–10 ms resulting in a local dryout region. The dryout region interrupts the otherwise continuous fluid flow and prevents the liquid flowing smoothly downstream. In the present work, multiple tests conducted at different flow and thermal conditions do not confirm the presence of a steady annular flow regime in our 120 μm hydraulic diameter microchannel.

The three-zone flow boiling model of Thome et al. [22] assumes that heat transfer events in the flow boiling process have a cyclic nature. The model further considers that heat transfer associated with the thin film evaporation region is typically on the order of several times that of the liquid slug while that for the vapor slug is nearly negligible [22]. These assumptions are consistent with the observations made in the benchmark experiments discussed earlier. To examine the model quantitatively, local heat transfer coefficients of the three-zone model and those of the current experiment (corresponding to the temperature and heat flux data of Fig. 5) are compared in Fig. 15. As it can be seen, the model well presents the cyclic variation in the heat transfer coefficient with time. However, the local heat transfer coefficients of the model are almost three times higher than the experimental data. This discrepancy between the experiment and the model is rooted in the relation employed to estimate the initial liquid film thickness. Also, duration of the thin film evaporation mode estimated by the model is almost half of that detected in the experiment. In addition, the experimental data show that toward the end of the dryout process, the local heat transfer coefficient rapidly

Table 1 A detailed breakdown of the magnitude of all heat transfer mechanisms and their relative contributions as a percentage of the total heat transfer during one cyclic passing of a liquid slug, an elongated bubble, and a partial dryout event (if it exists). The test is conducted at a mass flux of 68.4 kg/m^2 s, a frequency of 56 bubbles/s and an average temperature of 66 °C at the SU8–Si interface. TFE, THC, and SPC stand for thin film evaporation, transient heat conduction, and single-phase convection, respectively.

	Surface heat transfer (μJ)				% contribution of heat transfer mechanisms			
τ (ms)	TFE	THC	Partial dryout	SPC	TFE	THC	Partial dryout	SPC
1.4	2.2	2.3	—	9.3	16	17	—	67
3	5.7	3	—	8.1	34	18	—	48
5.3	11.2	3	—	6.5	54	14	—	32
7.4	13.6	1.3	0.3	5.6	65	6	1	28
10.4	13.6	1.3	0.9	3.9	69	7	5	19

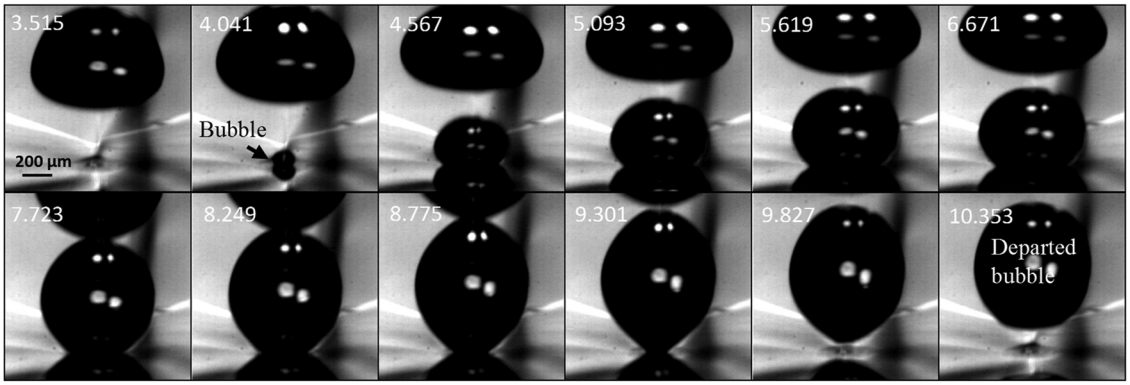

Fig. 13 Images of a nucleating bubble in pool boiling process at surface temperature 80.2 °C [17]

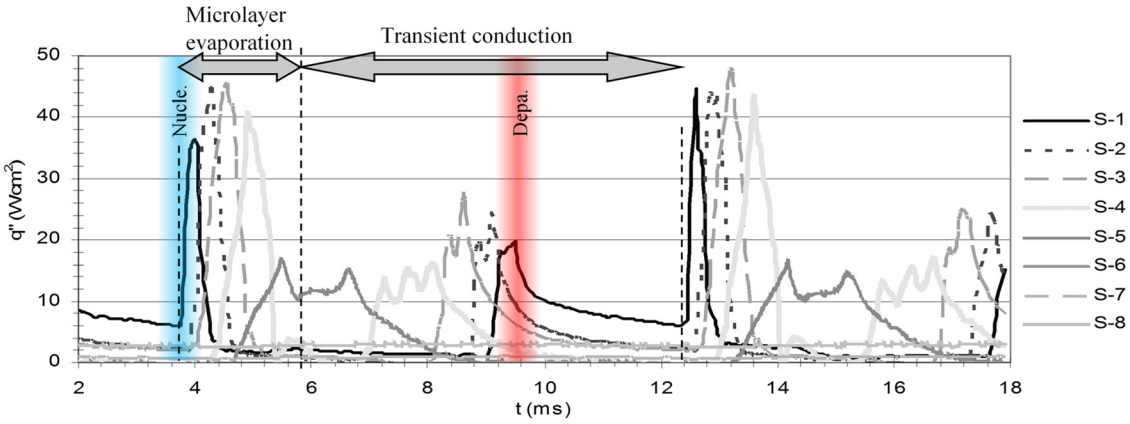

Fig. 14 Local heat flux variations corresponding to the bubble shown in Fig. 13 [17]

increases as the rear end of the bubble moves over and rewets sensor S26. The heat transfer associated with this process, known as the transient heat conduction mode of heat transfer, has not been included in the three-zone model.

5 Conclusions

A set of experiments were conducted to provide a microscopic level understanding of the heat transfer mechanisms in the microchannel flow boiling process. The experimental results revealed that four different regimes of heat transfer are active during the microchannel flow boiling process. These mechanisms are (1) microlayer and interline evaporation, (2) transient heat conduction, (3) partial dryout, and (4) single-phase convection. The magnitude and duration of these events depend on the bubble growth stage and generation frequency as follows:

(1) Upon nucleation of a bubble, the heat flux at the nucleation site spikes due to the microlayer/interline evaporation and transient conduction modes of heat transfer. The drag force acting on the bubble results in early departure of the bubble with an order of magnitude smaller departure diameter ($\sim$100 μm) than in the pool boiling process.
(2) As the bubble grows into a vapor slug and its contact area with the solid surface increases, the microlayer evaporation mechanism and its contribution to the overall surface heat transfer increases.
(3) When the vapor slug length substantially increases, the liquid layer between the vapor slug and surface partially dries out. The extent of the partial dryout depends on the initial thickness of the liquid film and the slug length.
(4) As a liquid front advances over (i.e., rewets) the bubble–surface contact area following the microlayer evaporation process, a sudden spike in heat flux occurs. This phenomenon arises from a mismatch between the surface and liquid temperatures as they come into contact. The physics of this process is consistent with what is considered as transient conduction mode of heat transfer that results

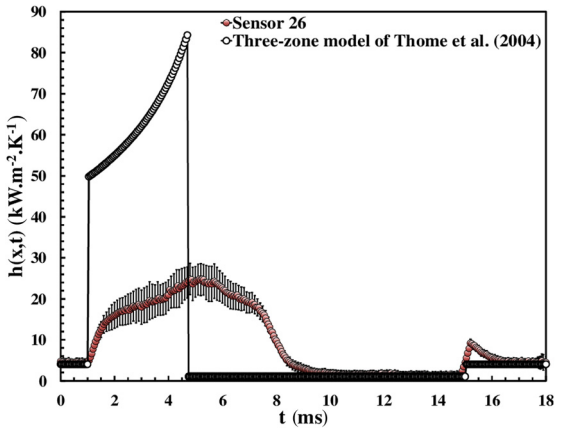

Fig. 15 Two-phase heat transfer coefficient-time histories measured at sensor 26 and calculated by the three-zone model [22]

from the rewetting of a hot surface with the cooler bulk liquid. This mechanism has a limited contribution to the overall surface heat transfer.

(5) At the end of the transient conduction process, when liquid fully rewets the surface, the local heat flux gradually declines and reaches to that of a single-phase convection process. The heat flux through this mechanism remains nearly constant for short liquid slugs. However, the surface heat flux associated with long liquid slugs slowly declines as the liquid temperature approaches the surface temperature.

(6) The surface heat transfer events associated with successive bubbles are temporally segregated at a low bubble generation frequency. Increasing the bubble generation frequency results in truncation or near complete circumvention of single-phase heat transfer events.

Bubbles nucleation does not cause any measurable enhancement in the single-phase convection heat transfer suggesting the absence of liquid agitation around nucleating bubbles. This contrasts the pool boiling heat transfer process in which departure of an order of magnitude of larger bubbles gives rise to microconvection heat transfer mechanism with a substantial contribution to the overall surface heat transfer. In light of these findings, care must be taken when extending the Jakob's [11] hypothesis to microchannels. Consistent with the microchannel flow boiling models based on the thin film evaporation, our experiments suggested that thin film evaporation is the most effective mechanism among various heat transfer mechanisms. However, under the test conditions presented here, a steady annular flow regime is absent. The microlayer disappears within 6–10 ms resulting in surface dryout. The thermal events observed are more consistent with the three-zone flow boiling model. However, the three-zone model fails to quantitatively predict the experimental results.

Acknowledgment

This study is supported by a grant from the National Science Foundation (NSF) under Contract No. CBET-1403657. Fabrication of the devices was conducted in the Nanoscale Research Facility (NRF) at the University of Florida.

References

[1] Li, D., Wu, G. S., Wang, W., Wang, Y. D., Liu, D., Zhang, D. C., Chen, Y. F., Peterson, G. P., and Yang R., 2012, "Enhancing Flow Boiling Heat Transfer in Microchannels for Thermal Management With Monolithically-Integrated Silicon Nanowires," Nano Lett., **12**, pp. 3385–3390.

[2] Thome, J. R., 2004, "Boiling in Microchannels: A Review of Experiment and Theory," Int. J. Heat Fluid Flow, **25**, pp. 128–139.

[3] Mudawar, I., 2011, "Two-Phase Microchannel Heat Sinks: Theory, Applications, and Limitations," ASME J. Electron. Packag., **133**(4), p. 041002.

[4] Bigham, S., and Moghaddam, S., 2015, "Microscale Study of Mechanisms of Heat Transfer During Flow Boiling in a Microchannel," Int. J. Heat Mass Transfer, **88**, pp. 111–121.

[5] Fazeli, A., Bigham, S., and Moghaddam, S., 2016, "Microscale Layering of Liquid and Vapor Phases Within Microstructures for a New Generation Two-Phase Heat Sink," Int. J. Heat Mass Transfer, **95**, pp. 368–378.

[6] Fazeli, A., Mortazavi, M., and Moghaddam, S., 2015, "Hierarchical Biphilic Micro/Nanostructures for a New Generation Phase-Change Heat Sink," Appl. Therm. Eng., **78**, pp. 380–386.

[7] Fershtman, A., Shemer, L., and Barnea, D., 2016, "Instantaneous Heat Transfer Rate Around Consecutive Taylor Bubbles," Int. J. Heat Mass Transfer, **95**, pp. 865–873.

[8] Scammell, A., and Kim, J., 2015, "Heat Transfer and Flow Characteristics of Rising Taylor Bubbles," Int. J. Heat Mass Transfer, **89**, pp. 379–389.

[9] Bandara, T., Nguyen, N.-T., and Rosengarten, G., 2015, "Slug Flow Heat Transfer Without Phase Change in Microchannels: A Review," Chem. Eng. Sci., **126**, pp. 283–295.

[10] Lee, P.-S., and Garimella, S. V., 2005, "Hot-Spot Thermal Management With Flow Modulation in a Microchannel Heat Sink," ASME Paper No. IMECE2005-79562.

[11] Jakob, M., 1949, *Heat Transfer*, Wiley, New York.

[12] Rohsenow, W. M., 1952, "Heat Transfer," Symposium, Engineering Research Institute, University of Michigan, Ann Arbor, MI, pp. 101–149.

[13] Chen, J. C., 1966, "Correlation for Boiling Heat Transfer to Saturated Fluids in Convective Flow," Ind. Eng. Chem. Process Des. Dev., **5**, pp. 322–329.

[14] Steiner, D., and Taborek, J., 1992, "Flow Boiling Heat Transfer in Vertical Tubes Correlated by an Asymptotic Model," Heat Transfer Eng., **13**, pp. 43–69.

[15] Kattan, N., Thome, J. R. R., and Favrat, D., 1998, "Flow Boiling in Horizontal Tubes—Part 3: Development of a New Heat Transfer Model Based on Flow Patterns," ASME J. Heat Transfer, **120**, pp. 156–165.

[16] Kandlikar, S. G., 1990, "A General Correlation for Saturated Two-Phase Flow Boiling Heat Transfer Inside Horizontal and Vertical Tubes," ASME J. Heat Transfer, **112**, pp. 219–228.

[17] Moghaddam, S., and Kiger, K., 2009, "Physical Mechanisms of Heat Transfer During Single Bubble Nucleate Boiling of FC-72 Under Saturation Conditions—I: Experimental Investigation," Int. J. Heat Mass Transfer, **52**, pp. 1284–1294.

[18] Kandlikar, S. G., and Balasubramanian, P., 2004, "An Extension of the Flow Boiling Correlation to Transition, Laminar, and Deep Laminar Flows in Minichannels and Microchannels," Heat Transfer Eng., **25**, pp. 86–93.

[19] Bertsch, S. S., Groll, E. A., and Garimella, S. V., 2009, "A Composite Heat Transfer Correlation for Saturated Flow Boiling in Small Channels," Int. J. Heat Mass Transfer, **52**, pp. 2110–2118.

[20] Harirchian, T., and Garimella, S. V., 2012, "Flow Regime-Based Modeling of Heat Transfer and Pressure Drop in Microchannel Flow Boiling," Int. J. Heat Mass Transfer, **55**, pp. 1246–1260.

[21] Qu, W., and Mudawar, I., 2003, "Flow Boiling Heat Transfer in Two-Phase Micro-Channel Heat Sinks—II: Annular Two-Phase Flow Model," Int. J. Heat Mass Transfer, **46**, pp. 2773–2784.

[22] Thome, J. R., Dupont, V., and Jacobi, A. M., 2004, "Heat Transfer Model for Evaporation in Microchannels—Part I: Presentation of the Model," Int. J. Heat Mass Transfer, **47**, pp. 3375–3385.

[23] Bigham, S., and Moghaddam, S., 2015, "Role of Bubble Growth Dynamics on Microscale Heat Transfer Events in Microchannel Flow Boiling Process," Appl. Phys. Lett., **107**, p. 244103.

[24] Yabuki, T., and Nakabeppu, O., 2010, "Study on Heat Transfer Mechanism of Isolated Bubble Nucleate Boiling With Mems Sensors," International Heat Transfer Conference (IHTC14), Washington DC, Aug. 8–13, pp. 1–7.

[25] Rao, S. R., Houshmand, F., and Peles, Y., 2014, "Transient Flow Boiling Heat-Transfer Measurements in Microdomains," Int. J. Heat Mass Transfer, **76**, pp. 317–329.

[26] Moghaddam, S., and Kiger, K., 2009, "Physical Mechanisms of Heat Transfer During Single Bubble Nucleate Boiling of FC-72 Under Saturation Conditions—II: Theoretical Analysis," Int. J. Heat Mass Transfer, **52**(5–6), pp. 1295–1303.

[27] Carey, V. P., 1992, *Liquid-Vapor Phase Change Phenomena: An Introduction to the Thermophysics of Vaporization and Condensation Processes in Heat Transfer*, Hemisphere Publishing, Washington, DC.

[28] National Instruments Corporation, 2006, "National Instrument SCXI-1581 User Manual," National Instruments Corporation, Austin, TX.

[29] Demiray, F., and Kim, J., 2004, "Microscale Heat Transfer Measurements During Pool Boiling of FC-72: Effect of Subcooling," Int. J. Heat Mass Transfer, **47**(14–16), pp. 3257–3268.

[30] Moghaddam, S., 2006, "Microscale Study of Nucleation Process in Boiling of Low-Surface-Tension Liquids," Ph.D. thesis, University of Maryland, College Park, MD.

[31] Moghaddam, S., and Kiger, K. T., Modafe, A., and Ghodssi, R., 2007, "A Novel Benzocyclobutene-Based Device for Studying the Dynamics of Heat Transfer During the Nucleation Process," J. Microelectromech. Syst., **16**, pp. 1355–1366.